

Development and validation of a computational multibody model of the elbow joint

Munsur Rahman^{1c}, Akin Cil^{23b}, Michael Johnson^{23b}, Yunkai Lu^{1a}
and Trent M. Guess^{*12a}

¹Department of Civil and Mechanical Engineering, University of Missouri-Kansas City,
5110 Rockhill Road, Kansas City, MO 64110, USA

²Department of Orthopaedic Surgery, University of Missouri-Kansas City,
2411 Holmes Street, Kansas City, MO 64108, USA

³Department of Orthopaedics, Truman Medical Centers, 2301 Holmes Street,
Kansas City, MO 64108, USA

(Received August 06, 2013, Revised July 31, 2014, Accepted August 05, 2014)

Abstract. Computational multibody models of the elbow can provide a versatile tool to study joint mechanics, cartilage loading, ligament function and the effects of joint trauma and orthopaedic repair. An efficiently developed computational model can assist surgeons and other investigators in the design and evaluation of treatments for elbow injuries, and contribute to improvements in patient care. The purpose of this study was to develop an anatomically correct elbow joint model and validate the model against experimental data. The elbow model was constrained by multiple bundles of non-linear ligaments, three-dimensional deformable contacts between articulating geometries, and applied external loads. The developed anatomical computational models of the joint can then be incorporated into neuro-musculoskeletal models within a multibody framework. In the approach presented here, volume images of two cadaver elbows were generated by computed tomography (CT) and one elbow by magnetic resonance imaging (MRI) to construct the three-dimensional bone geometries for the model. The ligaments and triceps tendon were represented with non-linear spring-damper elements as a function of stiffness, ligament length and ligament zero-load length. Articular cartilage was represented as uniform thickness solids that allowed prediction of compliant contact forces. As a final step, the subject specific model was validated by comparing predicted kinematics and triceps tendon forces to experimentally obtained data of the identically loaded cadaver elbow. The maximum root mean square (RMS) error between the predicted and measured kinematics during the complete testing cycle was 4.9 mm medial-lateral translational of the radius relative to the humerus (for Specimen 2 in this study) and 5.30 internal-external rotation of the radius relative to the humerus (for Specimen 3 in this study). The maximum RMS error for triceps tendon force was 7.6 N (for Specimen 3).

Keywords: elbow; biomechanics; multibody; ligament; cartilage

1. Introduction

*Corresponding author, Ph.D., E-mail: guesstr@missouri.edu

^a Ph.D., ^b M.D., and ^c M.S. Student

The human elbow joint is a unique joint that produces the complex motion of the forearm needed for positioning of the hand. By permitting elbow function humans can accomplish various activities in their daily life that makes them distinct from other mammals (Gonzalez *et al.* 1996). Unfortunately, this important joint is the second most commonly dislocated joint in adults (de Haan *et al.* 2011). Although uncommon, osteoarthritis of the elbow can cause severe pain, loss of mobility, and entire upper limb disability (Degreef and De Smet 2011). Comprehensive knowledge of the *in vivo* loading of elbow structures is essential in understanding biomechanical causes associated with elbow degenerative disease and injuries, and to find appropriate treatment. A better understanding of *in vivo* mechanical loads has implications for the development and progression of osteoarthritis and reduces the cost of treatment (Guess *et al.* 2010). But currently, measuring the *in vivo* ligament and tendon forces and cartilage contact pressures of the elbow during everyday activities is not possible. Computational multibody models can be a useful tool to predict tendon, ligament and contact forces. These models can enhance our understanding of elbow mechanics and tissue interactions during dynamic conditions and would provide valuable insight to the *in vivo* loading environment of the elbow joint (Guess 2012). Therefore, computational models of the elbow could help to improve the diagnosis, treatment and rehabilitation of post-traumatic injuries of the elbow. A validated model can be used as a biomechanical tool for patient-specific preoperative planning, computer-aided surgery, and computer-aided rehabilitation (Fisk and Wayne 2009).

Finite element analysis and multibody dynamics are the two main tools of formulating computational models in biomechanics (Gonzalez *et al.* 1996, Kwak *et al.* 2000, Lemay and Crago 1996, Li *et al.* 1999, Liacouras and Wayne 2007, Raikova 1992, Wismans *et al.* 1980). The finite element method is necessary for determination of strain within tissue but the resulting simulations are computationally expensive both in development time and simulation time. Multibody modeling is the primary tool used for musculoskeletal movement simulations and researchers have applied multibody models for specific applications such as predicting muscle contributions to joint moments, body segment motion, menisci effect in the knee, joint stability, prediction of joint contact areas and pressures, and ligament function (Donahue *et al.* 2002, Ferreira *et al.* 2011, Fisk and Wayne 2009, Guess 2012, Guess *et al.* 2013, Guess *et al.* 2010, Stylianou *et al.* 2012, Zielinska and Donahue 2006). Computational models that combine muscle forces and loading on joint structures during movement can be a valuable tool in orthopaedics (Guess 2012). Developing anatomical elbow models in the multibody framework for future use in musculoskeletal models of the upper extremities is the focus of this work.

Computational models of the elbow have been developed to investigate joint behavior (Buchanan *et al.* 1998, Fisk and Wayne 2009, Garner and Pandy 2001, Gonzalez *et al.* 1999, Gonzalez *et al.* 1996, Holzbaaur *et al.* 2005, Kwak *et al.* 2000, Lemay and Crago 1996, Raikova 1992, Schuind *et al.* 1991, Spratley and Wayne 2011, Triolo *et al.* 2001). Gonzalez *et al.* (1996) developed a computational elbow model to investigate the individual muscle force, relationship among muscle excitation patterns, and the effect of elbow position on the recruitment of individual muscles during ballistic movements. Lemay and Crago (1996) developed a dynamic model of the upper extremity that was capable of simulating elbow flexion-extension and forearm pronation-supination movement. Both of these models assumed the joint structure to be constrained by idealized joint motion (e.g. hinge joint) rather than true anatomical joint motion from cartilage contact. In addition, previous studies that have investigated the ligament effect on joint stability have not included wrapping of ligaments around bone and the non-linear ligament 'toe' region (Fisk and Wayne 2009, Spratley and Wayne 2011).

The purpose of this study was to develop and validate an anatomically correct computational elbow joint models that include representation of articular cartilage, multiple ligament bundles having a non-linear toe region, as well as wrapping around bone of the lateral ulnar collateral and annular ligaments. This study examined the effects of different ligament modeling methods on motion kinematics during elbow flexion-extension associated with forearm rotation. The models are validated by comparing the predicted humerus, radius, and ulna kinematics and passive triceps tendon forces to experimental values from identically loaded cadaver elbows.

2. Materials and Methods

2.1 Cadaver elbow measurements and testing

Three fresh frozen cadaver elbow specimens were used for this study (Table 1). Two elbows were imaged with computed tomography (CT) scans and one was imaged with magnetic resonance imaging (MRI) after thawing at room temperature for 24 hours. CT scans of the elbows were taken using a Syngo CT (Siemens, Siemens medical solutions, PA) 20108 version software with 8 allocated bits and fine resolution scan. The following parameters were used for CT imaging: Imaging frequency 63.68 Hz, slice thickness of 1.5 mm, spacing between slices 2 mm, 192 group lengths, and 3 samples per pixel. MRIs were acquired using a 1.5T Siemens machine with the following parameter: TR:13.64, TE:6.82 and image resolution 512×512 , slice thickness 1.5mm, spacing between slices 1.875 mm. Before imaging custom “localizers” were rigidly attached with titanium screws to each bone segment (humerus, ulna and radius) after limited incisions through the skin and soft tissues down to the bone paying attention not to damage joint capsule and ligaments. The localizers were constructed from ABS plastic and contained two perpendicular tubes that were packed with vaseline to assist in global coordinate registration later in the experiment (Stylianou *et al.* 2012). The elbows were dissected by a shoulder and elbow fellowship trained orthopedic surgeon after the medical imaging. All tissue was removed from the bone except the joint capsule, medial and lateral collateral ligaments and triceps, biceps and brachialis tendons.

After dissection, the cadaver elbows were mounted in a dynamic bi-axial mechanical tester (Bose 3510-AT, Bose Corporation, Framingham, MA). The humeral head was cemented inside a cylinder that was attached by a hinge joint to the top ram of the mechanical tester, which could only move in the vertical direction. In order to constrain the ulna, the radius was disarticulated from the distal radioulnar joint for Specimen 1 keeping the interosseous membrane partially intact (Fig. 1(a)). The ulna was then cemented to a cup that was connected to the bottom ram of the mechanical tester through a universal joint. The bottom ram could only rotate about a vertical axis. Rather than disarticulating the distal radio-ulnar joint for specimens 2 and 3, a 10 hole steel dynamic compression plate (Stryker, Mahwah, NJ) was used. In order to mount the ulna to the cup for these specimens without constraining the distal radio-ulnar joint, 4 titanium screws were applied through the holes of the plate while the rest of the plate was cemented into the cup (Fig. 1(b)). The radius was free from any extra mechanical constraint. The Triceps tendon was exposed and a suture was used to connect the tendon to a 100N load cell attached to the humerus cylinder. The brachialis and biceps tendons were not attached. An Optotrak Certus motion Capture system (Northern Digital Inc, Waterloo, Ontario, Canada) was used to track bone motion during each experiment. Four rigid-body ires (each containing three infrared markers (Fig. 1(a)) were

Table 1 Cadaver elbow information for this study

	Age at death (years)	Gender	Right or Left	Height (in)	Weight (lbs)
Specimen 1	61	Male	Left	68	160
Specimen 2	42	Male	Right	72	270
Specimen 3	44	Female	Left	60	93

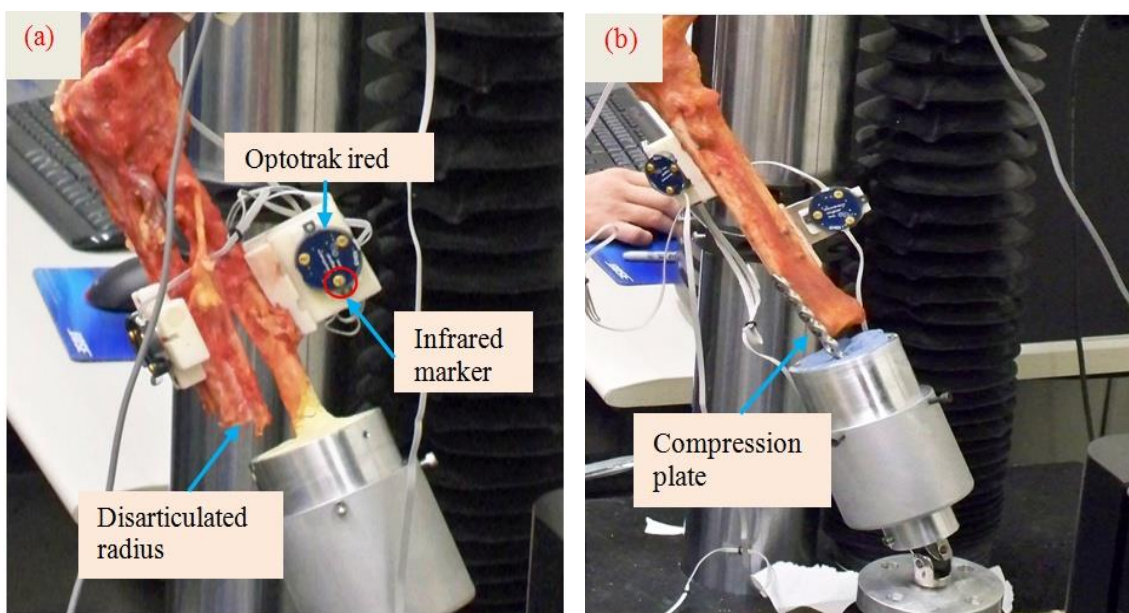


Fig. 1 (a) The radius was disarticulated from distal radioulnar joint and ulna is cemented directly to the cup for specimen 1. (b) A ten hole steel dynamic compression plate was used to constrain the ulna without disarticulating the radioulnar joint for specimens 2 and 3

attached to the humerus, radius, ulna, and humerus cylinder to track the kinematics of the bone segments. The initial position and orientation of cadaveric bone geometries relative to the mechanical tester were recorded using a probing tip of the Optotrak system.

A motion profile of 50 mm vertical displacement was applied to the top ram (25 mm downward from starting position and then 50 mm upward to reach maximum position). A rotation of 10 degrees (± 5 degrees from equilibrium position) was also applied to the bottom ram during testing (Fig. 2(a)). The approximate elbow flexion angle produced by this vertical motion for each specimen is given in Table 2. The flexion angles were determined by the humerus and ulna coordinate systems (as defined in Fig. 6). For each simulation, the three-dimensional coordinates of each infrared marker was recorded with the Optotrak Certus system. The forces on the triceps tendon were also recorded.

The kinematic envelope of motion (KEM) was measured for the elbow joint and used to calculate ligament bundle zero-load lengths (the lengths at which ligament bundles first become

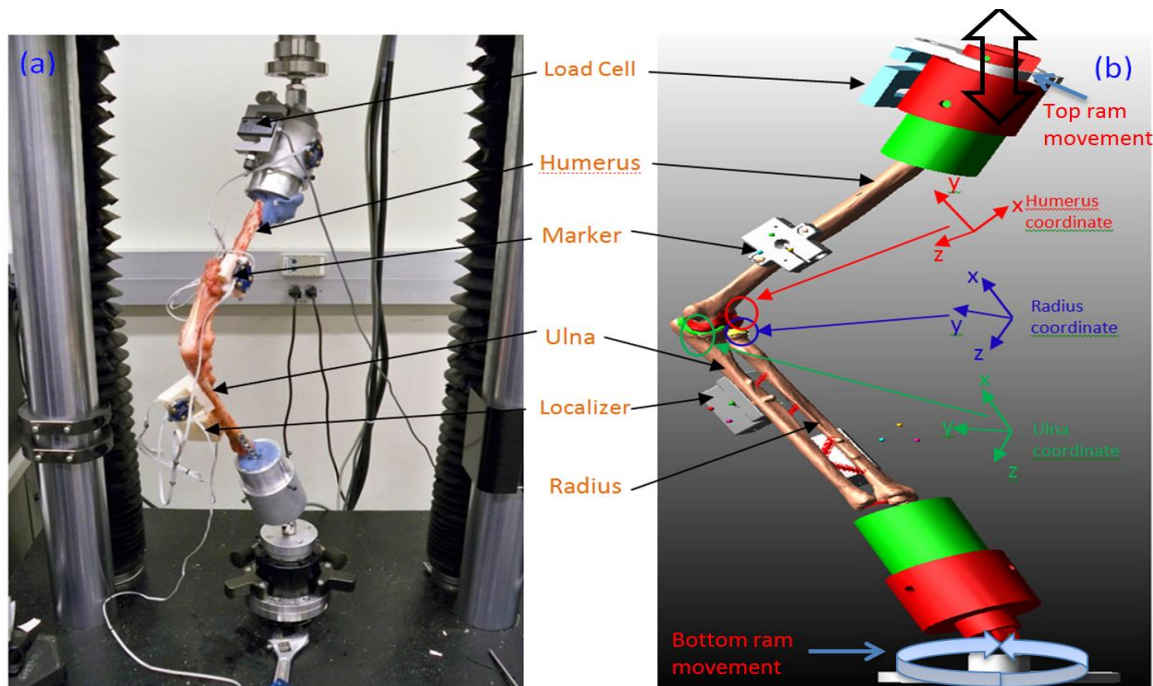


Fig. 2 (a) A cadaver elbow in the mechanical tester. (b) Multibody model of the elbow. The approximate position of the humerus, ulna, and radius coordinate system are also indicated by the circles

taut). For the KEM measurements, the humerus was held in a fixed position while the ulna was manually moved through its full range of motion with minimal force (as judged by the experimenter) (Guess *et al.* 2013). Bone motion was recorded by the attached Optotrak markers during this process. After all testing was completed, the elbow was dis-articulated and point clouds around the origin and insertion sites for the medial collateral ligament (MCL), lateral collateral ligament (LCL) complex, annular ligament, and triceps tendon were collected with an Optotrak digitizing probe. Additional points were also taken on the surface of the sigmoid notch, coronoid, olecranon, coronoid fossa, olecranon fossa, capitellum, trochlea, radial head, radial neck, bicipital tuberosity, and some on the diaphyses to assist in aligning the bones later in the model.

2.2 Multibody Model

Three-dimensional bone geometries of the humerus, ulna and radius were created from the two-dimensional Digital Imaging and Communications in Medicine (DICOM) files generated by Computed Tomography (CT) scan and Magnetic Resonance Imaging (MRI). The program 3D Slicer (www.slicer.org) was used to create the bone and localizer geometries by using auto thresholding from the CT scan images and manual segmentation from MRI. The 3D geometries were then imported to Geomagic Studio (Geomagic, Inc. Research Triangle Park, NC) for post-processing including smoothing, removing spikes, reducing noise, and decimation of the geometries to reduce file size. The cartilages were extracted as solid bodies of uniform thickness from the bones surface by using the feature available in Geomagic Studio. The geometries were then imported to the multibody modeling program Adams (MSC Software Corporation, Santa

Table 2 Elbow flexion angle during movement

	Initial flexion angle (deg)	Maximum flexion angle (deg)	Minimum flexion angle (deg)
Specimen 1	75	82	65
Specimen 2	91	96	86
Specimen 3	76	83	68

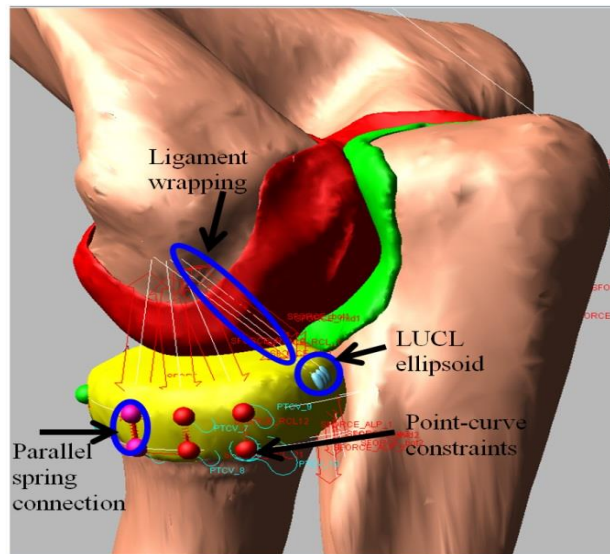


Fig. 3 Ligament wrapping of the LUCL and annular ligament around the bone. Also shown is the connection between two parallel elements of the LUCL and annular ligaments

Ana, CA) and aligned by using the initial position and point clouds of each bone collected during the cadaver testing (Fig. 2(b)).

The mass properties of each bone were defined from the geometries and a density of 1600 kg/m³ (Donahue *et al.* 2002). A density of 1000 kg/m³ was used for articular cartilage (Zielinska and Donahue 2006). Deformable contact constraints with no friction were defined between humerus and ulna, humerus and radius, ulna and radius, humerus cartilage and ulna cartilage, humerus cartilage and radius cartilage, ulna cartilage and radius cartilage using the modified Hertzian contact law:

$$F_c = k_c \delta^n + B_c(\delta) \dot{\delta} \quad (1)$$

where F_c is the contact force, δ is the interpenetration of the geometries, $\dot{\delta}$ is the velocity of interpenetration, k_c is the contact stiffness, n is the nonlinear power exponent, and $B_c(\delta)$ is a damping coefficient. To prevent discontinuities in the solution when the rigid bodies first make contact, the damping coefficient, $B_c(\delta)$, is a function of interpenetration (Hunt and Crossley 1975).

The ligament and tendons were attached to the model according to the insertion and origin point cloud information collected during experimental testing as identified by an orthopaedic surgeon. The ligaments were divided into bundles according to their structure and function. The model included three bundles for the medial collateral ligament (MCL) anterior part, three bundles for MCL posterior part, three bundles for the lateral ulnar collateral ligament (LUCL), three bundles for the radial collateral ligament (RCL) (Spratley and Wayne 2011), and two bundles for the annular ligament (Fisk and Wayne 2009). To simulate wrapping around bone, each ligament bundle of the LUCL and annular ligament was divided into multiple elements attached in series. For the annular ligament, small spheres were embedded in the ligament and a point-curve constraint defined between the spheres and line arcs placed along the perimeter of the radius head. The point-curve constraint allows the spheres to move along the path of the curves allowing the radius to rotate inside the ligament, similar to its physiological constraint (Fig. 3). For the LUCL, ellipsoids with a diameter equal to ligament thickness were embedded in the ligament. Deformable contacts using Eq. (1) were defined between the ellipsoids and radius cartilage. Parallel ligament elements of the LUCL and annular ligament were also connected with spring elements to restrain the elements from crossing each other (Fig. 3).

The ligaments and tendon were modeled as non-linear springs using a piecewise function describing the force-length relationship including the non-linear “toe” region (Fig. 4). The force-length for each ligament is described by Eqs. (2) and (3) (Blankevoort *et al.* 1991, Wismans *et al.* 1980).

$$f = \begin{cases} \frac{1}{4}k\varepsilon^2/\varepsilon_l & 0 \leq \varepsilon \leq 2\varepsilon_l \\ k(\varepsilon - \varepsilon_l) & \varepsilon > 2\varepsilon_l \\ 0 & \varepsilon < 0 \end{cases} \quad (2)$$

$$\varepsilon = \begin{pmatrix} l - l_0 \\ l \end{pmatrix} \quad (3)$$

where k is a stiffness parameter and ε is defined as an engineering strain (the ratio of range of motion divided by initial length (Eq. (3))). The stiffness parameter (k) is defined in units of force (N) and is derived from the stiffness coefficient (N/mm) by multiplying it by the ligament bundle zero load length (mm). The spring parameter ε_l is a constant value and it is assumed to be 0.03. A custom ADAMS subroutine was written to implement Eq. (2) in the model. Inputs to the subroutine include the ligament stiffness and strain, damping coefficient, the length of each ligament in the position it was constructed, and the measured zero-load length. The zero-load length, l_0 , for each ligament was determined by calculating the maximum straight-line distance between insertion and origin sites of the individual ligament throughout motion from the KEM test (Table 3). To account for the application of some force being applied to the bone during the KEM measurements, a correction factor of 80% was applied to each ligament bundle (Bloemker *et al.* 2012). Values of stiffness coefficient (α) (Table 3) for each ligament bundle came from (Fisk and Wayne 2009, Spratley and Wayne 2011, Regan *et al.* 1991). Each 1-D spring also included a parallel damper with a damping coefficient of 0.5 Ns/mm to remove the possibility of high frequency vibration during simulation (Guess 2012). The triceps tendon was modeled as a single

Table 3 Ligament model parameters.

Ligament Bundle	Description	Stiffness co-efficient (N/mm)	Zero-load length (mm)		
			Specimen 1	Specimen 2	Specimen 3
aLUCL	Lateral Ulnar Collateral Ligament, anterior bundle	19.0	28.3	36.4	34.2
cLUCL	Lateral Ulnar Collateral Ligament, central bundle	19.0	29.8	37.3	36.7
pLUCL	Lateral Ulnar Collateral Ligament, posterior bundle	19.0	34.3	38.5	38.8
aMCL	Medial Collateral Ligament, Anterior part, ant. bundle	24.1	18.3	25.1	18.3
cMCL	Medial Collateral Ligament, Anterior part, cent. bundle	24.1	19.2	24.6	18.0
pMCL	Medial Collateral Ligament, Anterior part, post. bundle	24.1	19.8	23.6	17.3
PBAB	MCL, Posterior part, ant. bundle	17.4	15.5	20.2	14.9
PBCB	MCL, Posterior part, cent. bundle	17.4	15.3	19.3	13.5
PBPB	MCL, Posterior part, post. bundle	17.4	15.6	22.9	15.7
aRCL	Radial Collateral Ligament, anterior bundle	15.5	18.4	22.5	15.2
cRCL	Radial Collateral Ligament, central bundle	15.5	17.6	21.7	14.5
pRCL	Radial Collateral Ligament, posterior bundle	15.5	18.3	22.6	14.2
ALAB	Annular Ligament, proximal bundle	28.5	-	-	-
ALPB	Annular Ligament, distal bundle	28.5	-	-	-

bundle non-linear spring element. The interosseous membrane and distal radioulnar joint ligament were modeled as five bundles and two bundles of linear spring elements respectively (Fig. 5). The stiffness coefficient and insertion points for the interosseous membrane and distal radioulnar joint ligament were obtained from literature (Fisk and Wayne 2009, Spratley and Wayne 2011), (Table 4).

Table 4 Stiffness properties of Interosseous membrane

Tissue part	Bundle name	Stiffness coefficient (N/mm)
Interosseous membrane	Accessory part, Distal bundle	18.9
	Accessory part, proximal bundle	18.9
	Central part, Distal bundle	65.0
	Central part, proximal bundle	65.0
	Distal oblique bundle	65.0
Distal radioulnar joint ligaments	Dorsal bundle	13.2
	Palmar bundle	11.0

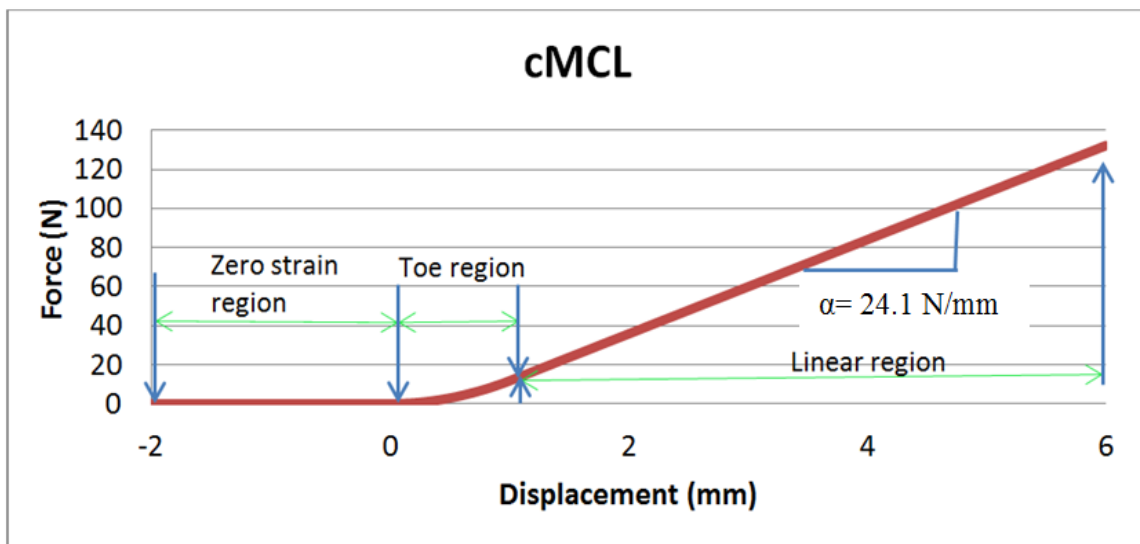


Fig. 4 The non-linear force-displacement relationship of the central bundle of the medial collateral ligament (cMCL) anterior part. The measured zero-load length of the cMCL was 17.2 mm and the stiffness coefficient (α) in the linear region was 24.1 N/mm

Local coordinate systems for each bone segment were created as described by Ferreira *et al.* (2011) and Morrey and Chao (1976). The Humerus, ulna, and radius coordinate systems were located at the point of capitellum center, center of the greater sigmoid notch, and radial head center respectively (Fig. 6). The X, Y and Z axes of the humerus coordinate system correspond approximately to the superior-inferior (S-I), anterior-posterior (A-P), and medial-lateral (M-L) directions respectively. The translations of the radius and ulna were computed from the origin of their respective local coordinate system relative to the humerus local coordinate system and were presented in humerus coordinates. The rotations were represented in a 123 Euler angle sequence

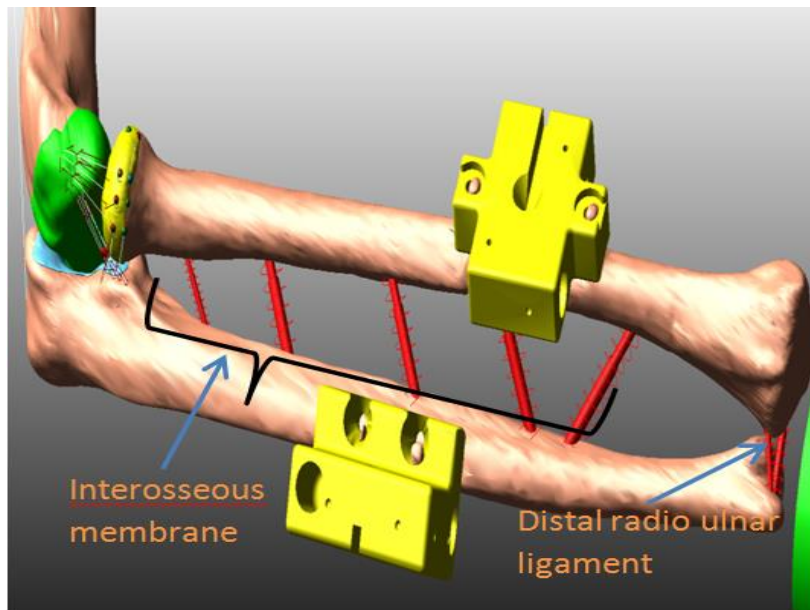


Fig. 5 Lateral view of model showing the interosseous membrane and distal radioulnar ligament of a right limb

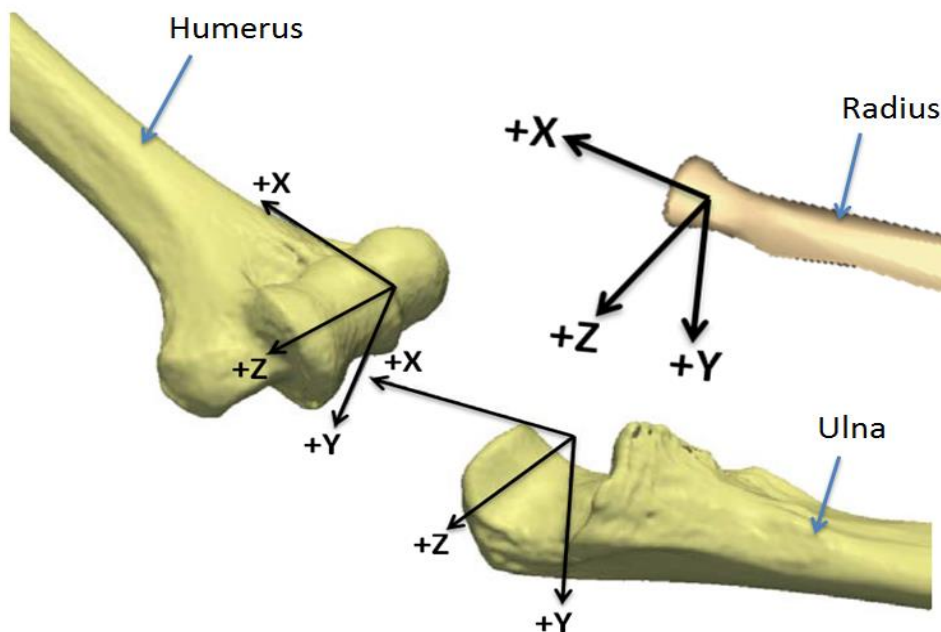


Fig. 6 Approximate position and orientation of the elbow joint local coordinate systems. The x-axis for the humeral coordinate system corresponds to the anterior-posterior (A-P) direction, the y-axis corresponds to the superior-inferior (S-I) direction, and the z-axis corresponds to the medial-lateral (M-L) direction as described by Ferreira *et al.* (2011) and Morrey and Chao (1976).

which correspond to internal-external rotation (I-E), varus-valgus (VR-VL), and flexion-extension (F-E). The model was then subjected to the same 50 mm vertical motion profile on the top ram and 100 axial rotations on the bottom ram as the cadaver experimental testing. Finally for each simulation, the kinematics of each segment along with the forces on the triceps tendon was predicted. Some additional simulations were also conducted to observe the kinematic difference for a linear-ligament and non-wrapping ligament assumption condition.

Analysis of variance (ANOVA) was conducted to examine the effect of ligament wrapping and ligament nonlinearity on model outputs. Kinematics RMS errors between experiment and predictions from the non-linear-wrapping model (the model that included both non-linear ligament and ligament wrapping) was taken as one sample for ANOVA calculations. Similarly, the kinematic RMS error between experiment and predictions from the non-wrapping model (the model that did not include ligament wrapping) was taken as the second data set. IBM SPSS (IBM Corporation, Armonk, NY, USA) statistics software was used to calculate the ANOVA from those two sets of data, and the F-ratios (the ratio of sample variances) were used to evaluate the significance of changing factors. A similar approach was followed for ANOVA calculations to compare the RMS error between non-linear-wrapping and the linear-ligament model (the model that did not include the ligament 'toe' region). The p-value was then used to measure the statistical significance and percentage confidence on the results. If the p-value was less than 0.05, then the factor was statistically significant for the result.

3. Results

Model predicted kinematics of the ulna and radius relative to the humerus were compared to experimental data (Figs. 7 and 8). Triceps tendon forces were also compared (Fig. 9). The RMS error (Table 5) between the experimental and predicted kinematics was calculated for all models in every ligament condition. RMS error was also calculated for the triceps tendon force for each model.

4. Discussion

The main aim of this study was to create and validate an anatomically correct subject specific computational multibody model of the elbow joint complex to predict joint biomechanical behavior. The models were developed in the multibody framework and can be placed in neuromusculoskeletal models of the arm for prediction of contact and ligament forces during movement. In addition, multibody modeling techniques can be applied that allow prediction of cartilage contact pressure during dynamic loading conditions as demonstrated by a recent study (Guess *et al.* 2013). Predicted bone kinematics were compared to experimental data from an identically loaded cadaver (Figs. 7 and 8). The largest translation RMS errors occurred in the medial-lateral direction for the radius relative to the humerus for all three specimens. Specimen 2 had the greatest translation errors with a maximum of 4.9 mm (Table 5). The maximum rotation RMS error was 5.30 internal-external rotation of the radius relative to the humerus for Specimen 3. The maximum RMS error for triceps tendon force was 7.6 N for Specimen 3 (Fig. 9). In most cases, the largest values of RMS error occurred for the radius coordinate system relative to the humerus coordinate system for all models.

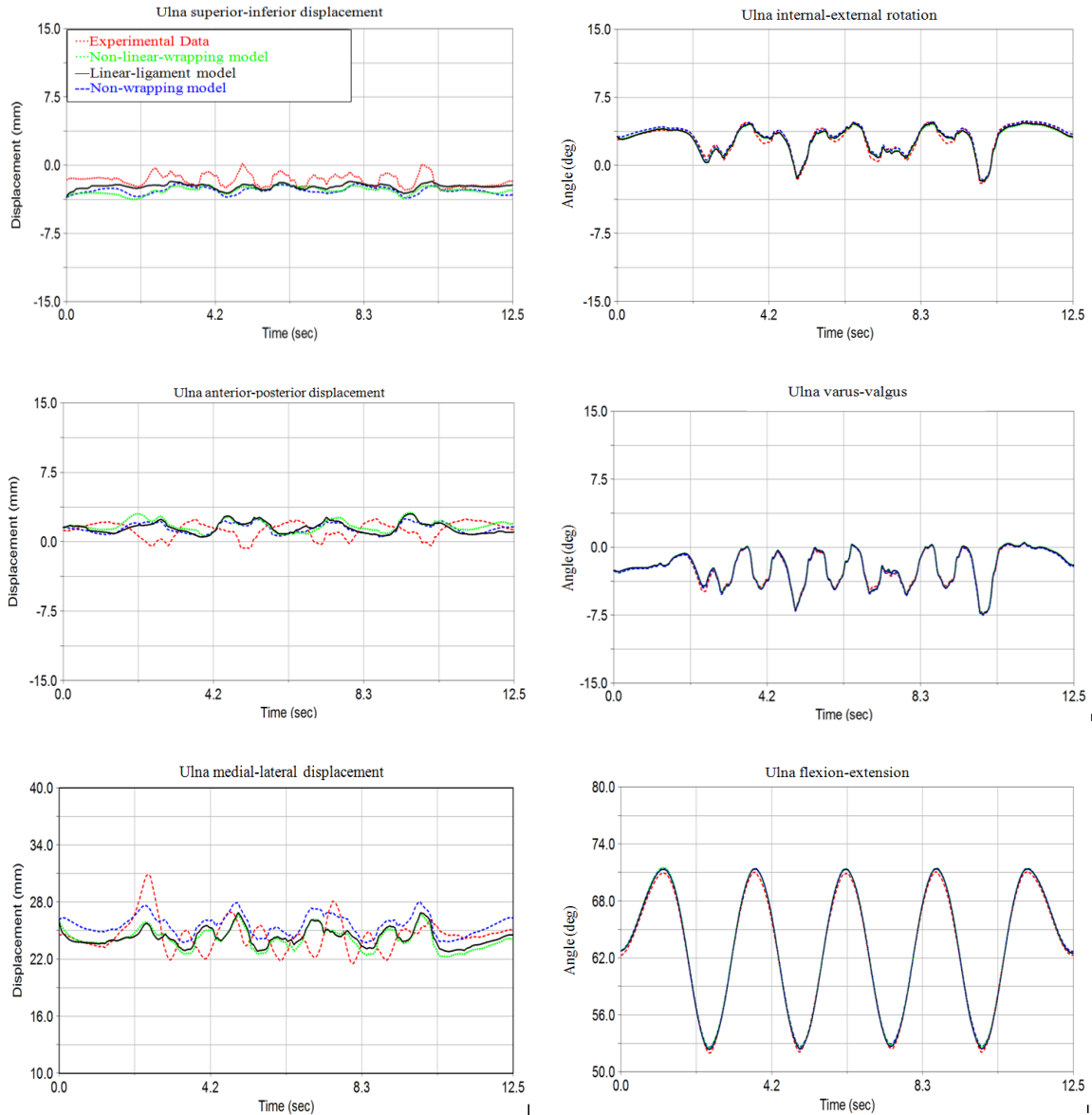


Fig. 7 Measured and predicted displacement and rotation of the ulna coordinate system relative to the humerus coordinate system for Specimen 1 during a 12.5 second simulation

Multiple sources of model and experimental error exist. During large rotations of the radius, the Optotrak cameras could lose sight of the ired markers, causing loss of kinematic data. Also, the articular cartilage geometries on bone surfaces were assumed to have a uniform thickness, but actual cartilage thickness is non-homogenous. As a result, the modeled contact surface will differ from the actual contact surfaces. This may affect contact magnitudes, locations and orientations, creating a source of modeling error. High quality MRI is recommended for future studies.

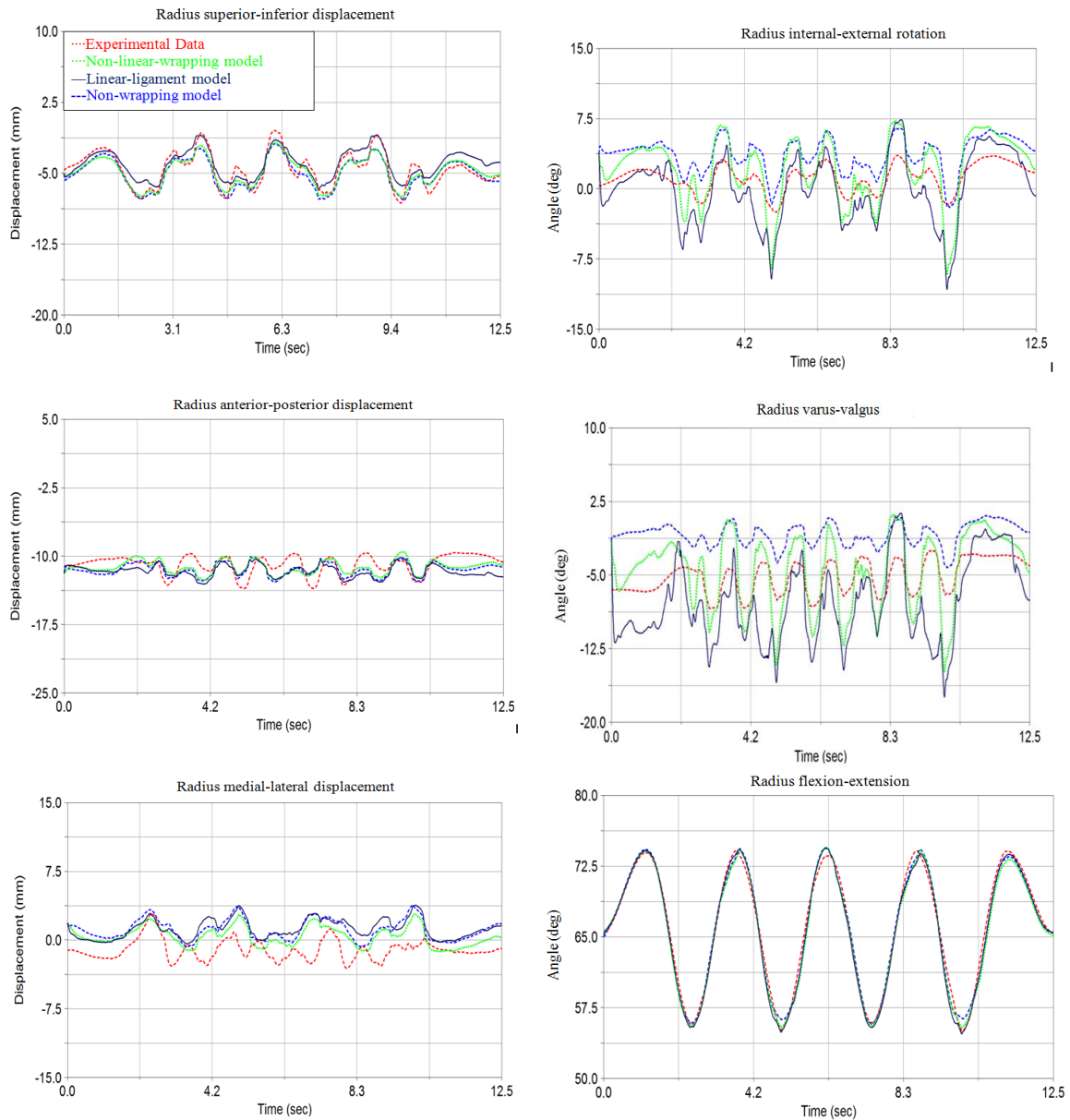


Fig. 8 Measured and predicted displacement and rotation of the radius coordinate system relative to the humerus coordinate system for Specimen 1 during a 12.5 second simulation

The model was validated only by testing the resulting segment motions and triceps tendon force. Contact forces and pressures in the cadaver elbow joint were not directly measured. In addition, the models were validated with only three cadavers. A larger sample size may help to make more generalized conclusions.

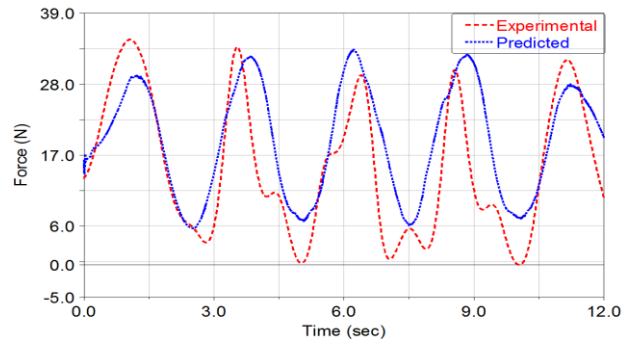


Fig. 9 Triceps tendon force comparison for Specimen 1

A limitation of rigid multibody models is that stress and strain within the tissue cannot be predicted. Predicting strain in cartilage and ligament tissues is important to understand tissue level degeneration and disease (Bei and Fregly 2004, Stylianou *et al.* 2012). Finally, the bi-axial mechanical tester had a limited range of motion (50 mm), producing small changes in flexion angle during experimental testing. A larger range of motion evaluating the elbow joint is important to understanding ligament characteristics. A larger flexion angle range is recommended for future studies. Specimen 1 was disarticulated from the distal radioulnar joint, reducing constraints for the radius and introducing unexpected movements. These limitations were overcome by using the steel dynamic compression plate for specimen 2 and 3. However, changes in predicted versus measured kinematics resulting from this change were small (Table 5).

Review of the literature revealed several modeling approaches for the elbow joint (Garner and Pandy 2001, Gonzalez *et al.* 1999, Gonzalez *et al.* 1996, Holzbaur *et al.* 2005, Lemay and Crago 1996, Raikova 1992, Triolo *et al.* 2001), but these models have typically ignored the ligament contribution in joint modeling. Although some models have incorporated the ligament effect and successfully predicted the elbow range of motion and varus-valgus laxities (Fisk and Wayne 2009, Spratley and Wayne 2011), modeling soft tissue, ligament non-linear property and ligament wrapping is a unique to the models presented in this work. The computational multibody model was able to represent flexion-extension associated with forearm rotation when compared to cadaver motion during testing. The model was also able to predict joint function by providing a more detailed description of the underlying structures. A small improvement in kinematics, compared to experimental measurements, was seen when a non-linear toe region was modeled in the ligament compared to models that had only a linear force-displacement relationship. Some reductions of RMS error were also observed when lateral ulnar collateral and annular ligament were wrapped around the bone. Although these observations were not statistically significant (ANOVA p-value was greater than 0.05), this may suggest that ligament toe region and ligament wrapping should be included. The ligament path was chosen for annular ligaments as a rigid spline that may resist the translational movement of the radius. The RMS error of the radius in medial-lateral translation was large compared to its overall range of motion. Including compliance in the ligament may improve the medial-lateral translation errors of the radius. Additional improvements to the model include using non-uniform discrete cartilage and adding more ligament wrapping. This modeling work is the first step in developing a musculoskeletal model of the elbow joint. The developed model will then be used for subject specific full musculoskeletal movement simulations of the upper-extremity.

Table 5 RMS errors between predicted and measured kinematics and triceps tendon forces for each elbow during each simulation. The maximum values for each axis are shown in bold

		Ulna Coordinate system						Radius Coordinate system					
		Displacement (mm)			Rotation (deg)			Displacement (mm)			Rotation (deg)		
		S-I	A-P	M-L	I-E	VR-VL	F-E	S-I	A-P	M-L	I-E	VR-VL	F-E
Specimen 1	Non-linear-wrapping	1.2	1.3	1.8	0.2	0.1	0.2	0.7	1.0	1.9	2.4	2.7	0.6
	Linear-ligament	0.8	1.3	1.8	0.6	0.1	0.2	1.0	1.3	2.6	2.7	4.2	0.7
	Non-wrapping	1.2	1.2	1.9	0.3	0.1	0.3	0.8	1.1	2.5	2.6	4.4	0.6
Specimen 2	Non-linear-wrapping	1.6	1.5	4.6	0.6	0.2	0.1	1.4	1.6	4.5	1.0	1.9	0.3
	Linear-ligament	1.8	1.5	4.6	0.6	0.2	0.2	1.1	1.8	4.9	1.0	1.9	0.1
	Non-wrapping	1.6	1.7	4.6	0.6	0.2	0.1	1.2	1.8	4.6	0.6	1.3	0.2
Specimen 3	Non-linear-wrapping	1.4	1.9	3.0	0.5	0.6	0.6	1.4	2.1	3.1	3.3	5.3	0.3
	Linear-ligament	1.1	1.9	3.0	0.4	0.5	0.5	1.3	2.1	3.4	3.3	5.3	0.5
	Non-wrapping	0.7	2.0	3.5	0.5	0.4	0.4	1.2	1.9	2.8	1.5	2.4	0.5
Triceps Tendon		Specimen 1 3.9			Specimen 2 2.6			Specimen 3 7.5					

Acknowledgments

This research was funded by the School of Medicine, University of Missouri-Kansas City (UMKC). The authors gratefully acknowledge the support of Dr. Kia and Dr. Stylianos from the Musculoskeletal Biomechanics Research Laboratory, UMKC, for their contributions to this project.

References

- Bei, Y., and Fregly, B.J. (2004), "Multibody dynamic simulation of knee contact mechanics", *Med. Eng. Phys.*, **26**(9), 777-789.
- Blankevoort, L., Kuiper, J.H., Huiskes, R., and Grootenboer, H. J. (1991), "Articular contact in a three-dimensional model of the knee", *J. Biomech.*, **24**(11), 1019-1031.
- Bloemker, K.H., Guess, T.M., Maletsky, L., and Dodd, K. (2012), "Computational knee ligament modeling using experimentally determined zero-load lengths", *Open Biomed. Eng. J.*, **6**, 33-41.
- Buchanan, T.S., Delp, S.L., and Solbeck, J.A. (1998), "Muscular resistance to varus and valgus loads at the elbow", *J. Biomech. Eng.*, **120**(5), 634-639.
- de Haan, J., Schep, N.W., Eygendaal, D., Kleinrensink, G.J., Tuinebreijer, W.E., and den Hartog, D. (2011), "Stability of the elbow joint: relevant anatomy and clinical implications of in vitro biomechanical studies", *Open Orthop. J.*, **5**, 168-176.
- Degreef, I., and De Smet, L. (2011), "The arthroscopic ulnohumeral arthroplasty: from mini-open to arthroscopic surgery", *Minim. Invasive Surg.*, 798084.
- Donahue, T.L., Hull, M.L., Rashid, M.M., and Jacobs, C.R. (2002), "A finite element model of the human knee joint for the study of tibio-femoral contact", *J. Biomech. Eng.*, **124**(3), 273-280.
- Ferreira, L.M., King, G.J., and Johnson, J.A. (2011), "Motion-derived coordinate systems reduce inter-subject variability of elbow flexion kinematics", *J. Orthop. Res.*, **29**(4), 596-601.
- Fisk, J. P., and Wayne, J.S. (2009), "Development and validation of a computational musculoskeletal model of the elbow and forearm", *Ann. Biomed. Eng.*, **37**(4), 803-812.
- Garner, B.A., and Pandy, M.G. (2001), "Musculoskeletal model of the upper limb based on the visible human male dataset", *Comput. Methods Biomech. Biomed. Eng.*, **4**(2), 93-126.
- Gonzalez, R.V., Abraham, L.D., Barr, R.E., and Buchanan, T.S. (1999), "Muscle activity in rapid multi-degree-of-freedom elbow movements: solutions from a musculoskeletal model", *Biol. Cybern.*, **80**(5), 357-367.
- Gonzalez, R.V., Hutchins, E.L., Barr, R.E., and Abraham, L.D. (1996), "Development and evaluation of a musculoskeletal model of the elbow joint complex", *J. Biomech. Eng.*, **118**(1), 32-40.
- Guess, T.M. (2012), "Forward dynamics simulation using a natural knee with menisci in the multibody framework", *Multibody Syst. Dyn.*, **28**(1-2), 37-53.
- Guess, T.M., Liu, H., Bhashyam, S., and Thiagarajan, G. (2013), "A multibody knee model with discrete cartilage prediction of tibio-femoral contact mechanics", *Comput. Methods Biomech. Biomed. Eng.*, **16**(3), 256-270.
- Guess, T.M., Thiagarajan, G., Kia, M., and Mishra, M. (2010), "A subject specific multibody model of the knee with menisci", *Med. Eng. Phys.*, **32**(5), 505-515.
- Holzbaur, K.R., Murray, W.M., and Delp, S.L. (2005), "A model of the upper extremity for simulating musculoskeletal surgery and analyzing neuromuscular control", *Ann. Biomed. Eng.*, **33**(6), 829-840.
- Hunt, K.H., and Crossley, F.R.E. (1975), "Coefficient of Restitution Interpreted as Damping in Vibroimpact", *J. Appl. Mech.*, **42**(2), 440.
- Kwak, S.D., Blankevoort, L., and Ateshian, G.A. (2000), "A Mathematical Formulation for 3D Quasi-Static Multibody Models of Diarthrodial Joints", *Comput. Methods Biomech. Biomed. Eng.*, **3**(1), 41-64.
- Lemay, M.A., and Crago, P.E. (1996), "A dynamic model for simulating movements of the elbow, forearm, an wrist", *J. Biomech.*, **29**(10), 1319-1330.
- Li, G., Gil, J., Kanamori, A., and Woo, S.L. (1999), "A validated three-dimensional computational model of a human knee joint", *J. Biomech. Eng.*, **121**(6), 657-662.
- Liacouras, P.C., and Wayne, J.S. (2007), "Computational modeling to predict mechanical function of joints: application to the lower leg with simulation of two cadaver studies", *J. Biomech. Eng.*, **129**(6), 811-817.
- Morrey, B.F., and Chao, E.Y. (1976), "Passive motion of the elbow joint", *J. Bone Joint Surg. Am.*, **58**(4), 501-508.
- Raikova, R. (1992), "A general approach for modelling and mathematical investigation of the human upper

- limb”, *J. Biomech.*, **25**(8), 857-867.
- Regan, W.D., Korinek, S.L., Morrey, B.F., and An, K.N. (1991), “Biomechanical study of ligaments around the elbow joint”, *Clin. Orthop. Relat. Res.*, **271**, 170-179.
- Schuind, F., An, K.N., Berglund, L., Rey, R., Cooney, W.P., 3rd, Linscheid, R.L., and Chao, E.Y. (1991), “The distal radioulnar ligaments: a biomechanical study”, *J. Hand Surg. Am.*, **16**(6), 1106-1114.
- Spratley, E.M., and Wayne, J.S. (2011), “Computational model of the human elbow and forearm: application to complex varus instability”, *Ann. Biomed. Eng.*, **39**(3), 1084-1091.
- Stylianou, A.P., Guess, T.M., and Cook, J.L. (2012), “Development and validation of a multi-body model of the canine stifle joint”, *Comput. Methods Biomech. Biomed. Eng.*, doi: 10.1080/10255842.2012.684243
- Triolo, R.J., Werner, K.N., and Kirsch, R. F. (2001), “Modeling the postural disturbances caused by upper extremity movements”, *IEEE Trans. Neural. Syst. Rehabil. Eng.*, **9**(2), 137-144.
- Wismans, J., Veldpaus, F., Janssen, J., Huson, A., and Struben, P. (1980), “A three-dimensional mathematical model of the knee-joint”, *J. Biomech.*, **13**(8), 677-685.
- Zielinska, B., and Donahue, T. L. (2006), “3D finite element model of meniscectomy: changes in joint contact behavior”, *J. Biomech. Eng.*, **128**(1), 115-123.

MC